Self-assembled nanoscale biosensors based on quantum dot FRET donors

IGOR L. MEDINTZ[1], AARON R. CLAPP[2], HEDI MATTOUSSI*[2], ELLEN R. GOLDMAN[1], BRENT FISHER[3] AND J. MATTHEW MAURO*[1,4]

[1]Center for Bio/Molecular Science and Engineering, Code 6910, US Naval Research Laboratory, Washington, DC 20375, USA
[2]Division of Optical Sciences, Code 5611, US Naval Research Laboratory, Washington, DC 20375, USA
[3]Department of Chemistry, Massachusetts Institute of Technology, Cambridge, Massachusetts 02139, USA
[4]Present address: Molecular Probes Inc., 29851 Willow Creek Road, Eugene, Oregon 97402, USA
*e-mail: hedimat@ccs.nrl.navy.mil; matt.mauro@probes.com

Published online: 24 August 2003; doi:10.1038/nmat961

The potential of luminescent semiconductor quantum dots (QDs) to enable development of hybrid inorganic-bioreceptor sensing materials has remained largely unrealized. We report the design, formation and testing of QD–protein assemblies that function as chemical sensors. In these assemblies, multiple copies of *Escherichia coli* maltose-binding protein (MBP) coordinate to each QD by a C-terminal oligohistidine segment and function as sugar receptors. Sensors are self-assembled in solution in a controllable manner. In one configuration, a β-cyclodextrin-QSY9 dark quencher conjugate bound in the MBP saccharide binding site results in fluorescence resonance energy-transfer (FRET) quenching of QD photoluminescence. Added maltose displaces the β-cyclodextrin-QSY9, and QD photoluminescence increases in a systematic manner. A second maltose sensor assembly consists of QDs coupled with Cy3-labelled MBP bound to β-cyclodextrin-Cy3.5. In this case, the QD donor drives sensor function through a two-step FRET mechanism that overcomes inherent QD donor–acceptor distance limitations. Quantum dot–biomolecule assemblies constructed using these methods may facilitate development of new hybrid sensing materials.

Development of robust, sensitive and reusable environmental sensors is a strong current scientific priority. As such, recognition-based biosensors capable of specifically detecting chemicals, toxins and bio-agents in their environment are under active development in many laboratories[1–5]. An important goal in biosensor evolution is production of nanoscale assemblies capable of continuously monitoring concentrations of target species in a simple, reliable manner. This is accomplished by designing sensor components to carry out analyte recognition and binding while simultaneously producing useful output signals through an integrated signal transduction system[1–6]. Optically addressed biosensors of this type often use fluorescence resonance energy transfer (FRET) in signal transduction. FRET has been used in carefully designed sensing systems for proteins, peptides, nucleic acids and small molecules[1–6].

A crucial aspect of FRET biosensor development involves optimizing energy donor and acceptor dyes to function in concert with desired recognition elements[1,3–5]. Although organic dyes are available to accomplish this, many have functional limitations such as pH dependence, susceptibility to photobleaching, and narrow excitation bands coupled with broad emission bands, all of which can compromise sensor performance. Recent advances in luminescent colloidal semiconductor nanocrystals or quantum dots (QDs) technology have expanded the range of potentially useful fluorophores in FRET-based sensing applications[7–11]. QDs (CdSe or CdTe) have broad excitation and size-tunable photoluminescence (PL) spectra with narrow emission bandwidths (full-width at half-maximum of ~25–45 nm) that span the visible spectrum, allowing simultaneous excitation of several particle sizes at a single wavelength. QDs also have exceptional photochemical stability and relatively high quantum yields[7–12,13]. If fully exploited, these unique QD properties, unmatched in any available organic fluorophore, will allow development of FRET-based nanoscale assemblies capable of continuously monitoring target (bio)chemical species in diverse environments.

Since the introduction of biocompatible QDs, the number of biotechnologically relevant applications reported for these versatile materials has grown rapidly[7–16]. Although most applications to date have focused on using QDs as protein- or DNA-conjugated fluorometric labels for cellular imaging, in immunoassays, or entrapped in polymer

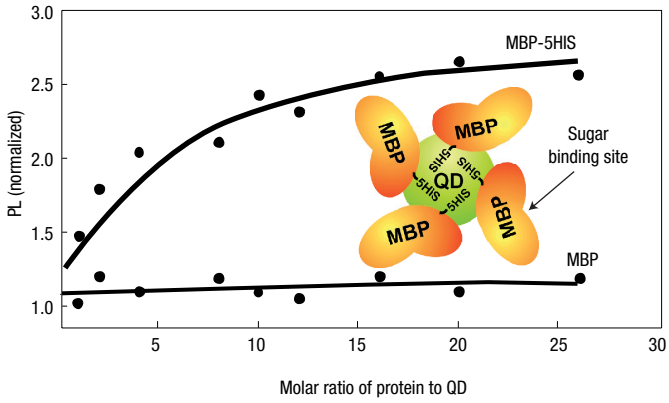

Figure 1 Comparison of the ability of MBP-5HIS (C-terminal penta-histidine) to coordinate with QDs as compared with MBP (minus the penta-histidine). The indicated molar ratio of protein to 560QD was allowed to coordinate and then assayed fluorimetrically. Photoluminescence (PL) is normalized to the QD emission intensity with no bound protein for comparison. Inset, cartoon of the QD-MBP-5HIS sensor assembly (here, and subsequently, reference to MBP implies the MBP-5HIS protein). The relative dimensions of QD to MBP are approximately to scale. A 530-nm QD (green), ~27–30 Å in size, with MBP molecules (orange) attached to the surface by Zn-pentahistidine coordination is shown. From 12–15 MBPs can occupy the available Zn coordination sites on the QD surface. The 560QD has a radius of 29–33 Å.

beads for optical barcoding, preliminary reports of QD–QD and QD–dye-labelled biomolecule FRETs have appeared[17–21]. In the present work, we have developed prototype nanosensors that take advantage of several of the physical and optical properties of protein-derivatized QDs for use in FRET-based chemical assays. We introduce several aspects of molecular receptor–QD assemblies that render them uniquely suitable for optical biosensing applications, as well as consider some of their inherent limitations and the potential means to overcome them.

For use as donors for FRET-based prototype QD sensor assemblies, we began with CdSe–ZnS core–shell nanocrystals (maximum emission wavelength, λ_{max} = 530 or 560 nm) rendered aqueous-compatible by an organic monolayer of dihydrolipoic acid attached to their ZnS shell through thiol coordination, referred to as DHLA-QDs[7,14]. As biorecognition elements, engineered variants of *Escherichia coli* maltose-binding protein (MBP), a well-characterized member of the bacterial periplasmic binding protein superfamily, were used. MBP has proven to be a versatile tool in prototyping nanosensor assemblies, including redox-active bioelectronic sensors[6], 'reagentless' or 'direct' recognition-based sensors[5,22,23], and recently, an elegant three-part GFP-MBP-ECFP fusion protein FRET sensor[24]. For achieving signal transduction in model energy-transfer assays, we prepared covalent β-cyclodextrin-acceptor dye conjugates (β-CD dyes) capable of binding within the saccharide-binding pocket of MBP and competing effectively with maltose, MBP's preferred substrate[2,22,23,25].

As Förster energy transfer is generally most efficient when the distance between donors and acceptors is in the 20–60 Å range[26], design considerations involved anchoring the protein receptor as close as possible to energy-donating QD cores to maximize FRET. Encapsulation of metal sulphide clusters by synthetic cognates of natural histidine-rich peptides suggested that a similar strategy might work for the present task[27]. To accomplish this, a variant of MBP expressed with a pentahistidine segment at its C-terminus (MBP-5HIS) was used for coordinative conjugation of the protein to QD surfaces. Figure 1 shows the results of fluorimetric titrations of 560 nm DHLA-QDs with either native MBP or MBP-5HIS over an identical range of protein-to-QD ratios. We previously demonstrated that the enhanced PL that occurs on binding of negatively charged DHLA-QDs with strongly positively charged protein domains is a reliable indicator of protein–QD interaction[7,10,11,14]. Other groups have reported this effect and even used it quantitatively[17,28–30]. Here, analogous behaviour is observed in QD titrations with MBP-5HIS; apparent saturation of the QD surface occurs at an average coverage of 12–15 proteins per 560-nm-emitting QD. The graphic inset in Fig. 1 schematically depicts a QD conjugated with ~12–15 MBP-5HIS proteins that would exhibit characteristically enhanced PL compared with an unconjugated QD (see also Fig. 2c). The observation that no PL enhancement occurs on QD titration with the identical MBP protein lacking the 5-HIS extension is convincing evidence that this C-terminal 5-HIS segment is responsible for immobilizing the protein on the QD ZnS–DHLA surface. Ligand competition studies in which imidazole competed with MBP-5HIS for QD binding provided additional evidence for protein binding through metal–histidine coordination (Supplementary Information, Fig. S1a). In addition, binding of QD–MBP-5HIS assemblies to a crosslinked amylose affinity matrix occurs through specific MBP–amylose interactions (Supplementary Information, Fig. S1B). Bound QD–protein assemblies can be subsequently eluted with excess maltose; QDs incubated with MBP lacking the 5HIS extension do not bind and elute from amylose matrix.

Although we surmise that coordination of the oligohistidine with QDs occurs at discontinuities or defects within the DHLA surface coating, details of both the PL enhancement mechanism and oligohistidine–QD coordination mode(s) remain to be elucidated. Carrying out QD–MBP–5HIS conjugation in this way allowed immobilization of multiple protein molecules directly onto the nanocrystal surfaces to yield unique prototype FRET sensor assemblies. Using smaller 530-nm-emitting QDs, we have observed identical PL surface-saturation effects, and have verified the ~10:1 protein/nanocrystal stoichiometry obtained from PL measurements using quantitative spin-dialysis methods (see Supplementary Information). The increased PL that occurs on protein binding to QD surfaces will potentially result in better optical efficiency and sensor performance, because the quantum yield typically increases 50 to 300% on QD surface saturation (the magnitude varies with each QD preparation).

The simpler of the two QD–MBP sugar-sensing nanoassemblies constructed consisted of 560-nm donor QDs (initial quantum yield ~15.6%), each conjugated with an average of 10 MBP-5HIS (subsequently referred to as MBP; quantum yield rises to ~39%) with their saccharide binding sites occupied by the displaceable β-CD-QSY9 energy acceptor dye signal transducing conjugate (Fig. 2a). The excellent overlap between QD emission and QSY9 absorption (Förster distance, R_0, 56.5 Å) allows β-CD-QSY9 bound within the MBP sugar-binding pocket to quench QD emission by ~50% (Fig. 2b,c). Quenching efficiency is improved by the presence of ~10 MBP per QD, each of which is capable of specifically binding a β-CD-QSY9 energy acceptor, compared with complexes with a single donor–acceptor FRET pair[26]. Increasing the number of energy acceptors per QD donor increases the effective acceptor extinction coefficient, which in turn proportionally improves the effective overlap integral for single QD donor–multiple acceptor complexes[26]. As MBP has a similar binding affinity for β-CD (1.80 μM) and maltose (3.50 μM) within its sugar-binding pocket[31], added maltose readily competes with and displaces the β-CD-QSY9 quencher, resulting in a concentration-dependent increase in QD PL, that is, quantitative maltose sensing (Fig. 2d). Using the conditions described in the Methods, an apparent dissociation constant, K_{app}, for maltose of 6.9 ± 0.2 μM (n = 3 experiments) was obtained using data derived from the increase in QD emission that occurs due to β-CD-QSY9 displacement (Fig. 2e)[24]. This 560QD-10MBP-β-CD-QSY9 nanosensor assembly was tested for its response to several different sugars at two concentrations. Only those containing the

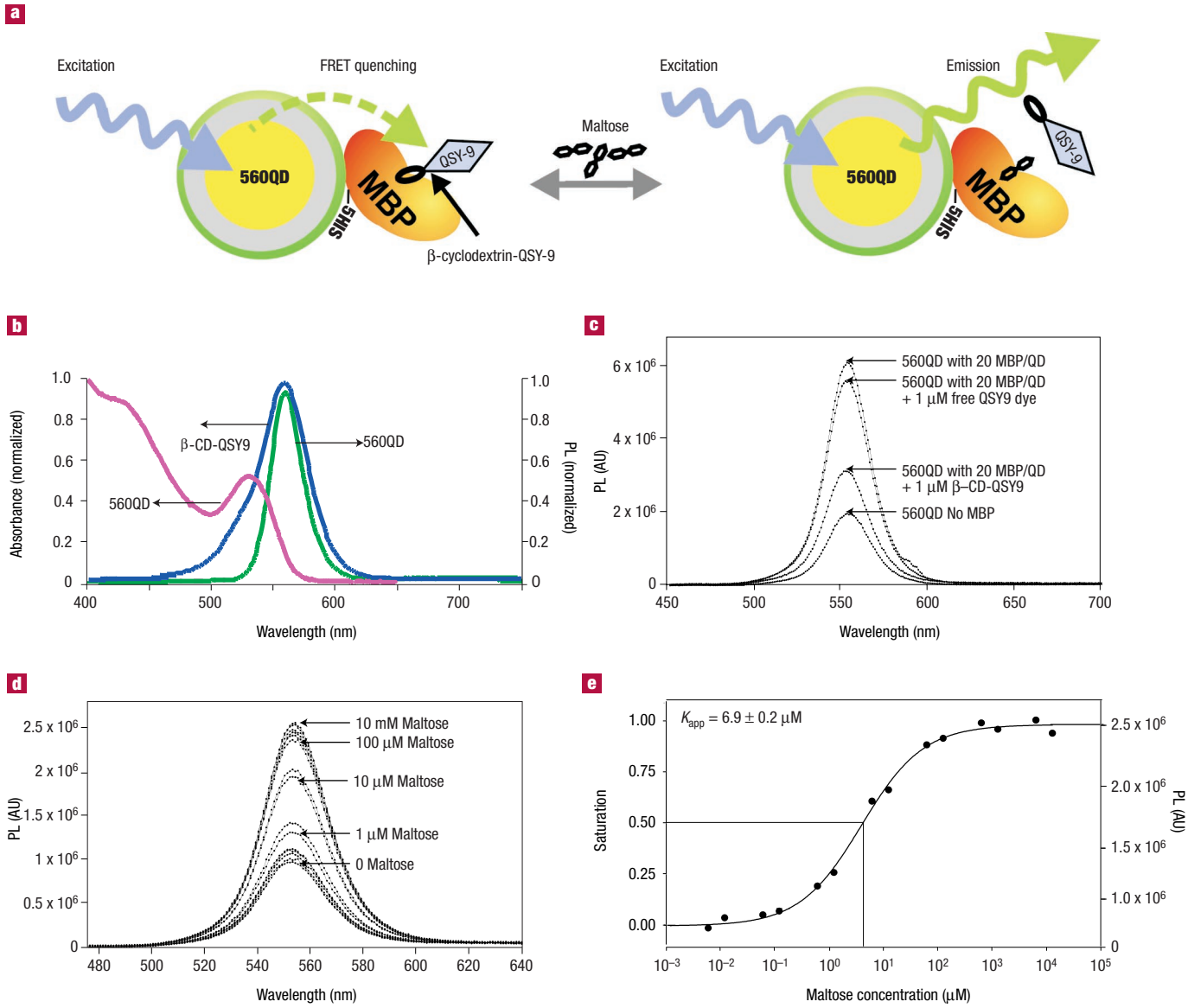

Figure 2 Function and properties of the 560QD-MBP nanosensor. a, 560QD-MBP nanosensor function schematic. Each 560-nm-emitting QD is surrounded by an average of ~10 MBP moieties; a single MBP is shown for simplicity. Formation of QD-MBP-β-CD-QSY9 (maximum absorption ~565 nm) results in quenching of QD emission. Added maltose displaces β-CD-QSY9 from the sensor assembly, resulting in an increase in direct QD emission. **b**, Spectral properties of 560QD-MBP sensor. Absorption (pink) and emission spectra (green) of MBP-conjugated 560QD are displayed along with the absorption spectra (blue) of β-CD-QSY9. Samples were excited at 400 nm and emission spectra recorded from 420 nm to 750 nm. Arrows indicate the reference axis. **c**, Demonstration of 560QD-MBP FRET quenching. PL spectra (AU = arbitrary units) were collected from 560QDs and 560QDs mixed with an average of 20 MBP/QD (saturated for effect). Note the resulting increase in PL (~300%). These same QD-MBP conjugates were then mixed with either 1 μM free QSY9 dye or 1 μM β-CD-QSY9. **d**, 560QD-10MBP maltose sensing. Titration of a 560QD-10MBP/QD conjugate (quantum yield ~39%) preassembled with 1 μM β-CD-QSY9 with increasing concentrations of maltose. **e**, Transformation of titration data. The right axis shows PL at 560 nm and fractional saturation is shown on the left axis. The point corresponding to 50% saturation was used to derive the maltose apparent dissociation constant (K_{app}) value. Assuming a range of useful measurement to be between 10 and 90% saturation translates into a sensing range of ~500 nm to 100 μM maltose[24].

α-1,4-glucosidic linkage elicited a significant response (Supplementary Information, Table S1). Thus, MBP attached to QD surfaces retains its specificity for recognizing and binding the α-1,4-glucosidic linkage.

Changes in QD excited-state lifetime for the 560QD-10MBP/QD-β-CD-QSY9 system (± maltose) parallel the results of the steady-state PL intensity measurements (Fig. 3a,b). The average lifetime (τ) for the 560QD-10MBP of ~8 ns decreases to 2.7 ns when β-CD-QSY9 occupies assembly MBP sugar-binding sites. Most importantly, addition of excess maltose, with resulting displacement of β-CD-QSY9, results in nearly full recovery of the donor lifetime (τ ~7.3 ns) (Fig. 3a,b). No effect on QD lifetimes was found in control experiments where maltose or β-CD was incubated with 560QD-10MBP assemblies alone (data not shown). Although unambiguous assignment of the quenching mechanism observed is impossible because QSY9 is a non-emitting quencher, we believe the combination of favourable donor–acceptor overlap integral and reversible sensing behaviour, based on specific competition for

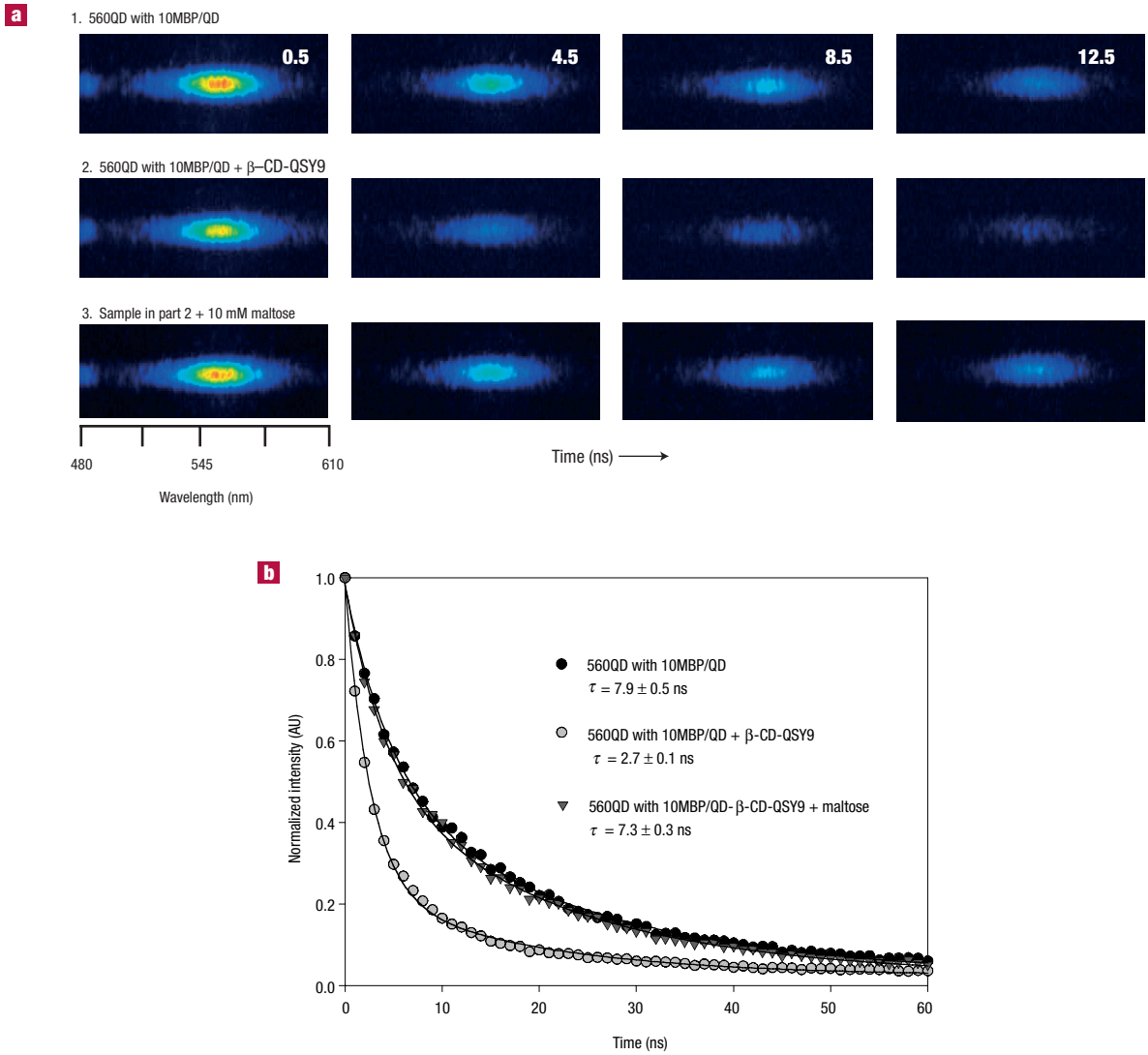

Figure 3 Excited-state properties of the 560QD-MBP nanosensor. a, False colour time-intensity-wavelength images of 560QD-10MBP nanosensor PL excited-state lifetime intensity. Images were collected of each indicated assembly at the indicated time points (upper right corner) following the laser excitation pulse. Image panel **1**: 560QD with 10MBP/QD. Panel **2**: 560QD with 10MBP/QD preloaded with 1 μM β-CD-QSY9. Panel **3**: the sample in panel **2** after addition of 10 mM maltose. The indicated emission wavelength scale is for all panels (intensity: black = 0; blue = lowest; red = highest). **b**, Fluorescence lifetime decay curves and τ values (at λ max) of 560QD-10MBP/QD sensor assemblies presented in **a**.

binding to the MBP sugar-binding site, makes it highly likely that FRET is the major quenching effect in this assembly. Additionally, this sensor assembly has the practical advantage of transducing sugar binding into an optical signal in a desirable 'switch on' mode in which analyte binding results in a direct increase in QD PL.

A potential limitation of using QD donors for FRET-based optical sensors involves the physical dimensions of nanocrystals compared to organic dye or metal chelate energy donors. For a CdSe–ZnS core–shell QD emitting at 530 nm, the closest approach a surface-bound energy acceptor can make to the QD core is 27–30 Å (this estimate ignores any effect the DHLA cap might have on the acceptor approach distance). Use of an intervening 'optical relay station' or 'midway fluorophore' to accomplish step-wise energy transfer over long distances has been demonstrated in DNA oligomer–dye systems[32,33]. To obviate distance limitations imposed as a result of QD size, we designed and prepared a two-step FRET QD-MBP sugar-sensing assembly containing a fluorescent dye acting as a relay station. In this assembly, each 530-nm QD donor (quantum yield ~10.6%, with 10 MBPs ~15%) was conjugated with 10 Cy3-labelled MBP molecules. The protein-bound Cy3 served as a bridging acceptor/donor for ultimate energy transfer to maltose-displacable β-CD-Cy3.5 bound at MBP saccharide binding sites (Fig. 4a,b). For nanosensor homogeneity, we used a single-cysteine MBP variant (D95C) that was site-specifically labelled at the cysteine with thiol-reactive Cy3 dye[23]. Titration of these QDs with increasing amounts of Cy3-labelled MBP showed efficient quenching of QD emission, ~95% quenching at 10:1 dye/QD ratio (Fig. 4c). Concomitant systematic increases in Cy3 emission due to increasing QD/protein-bound-Cy3 energy transfer occurred. Using the FRET titration data

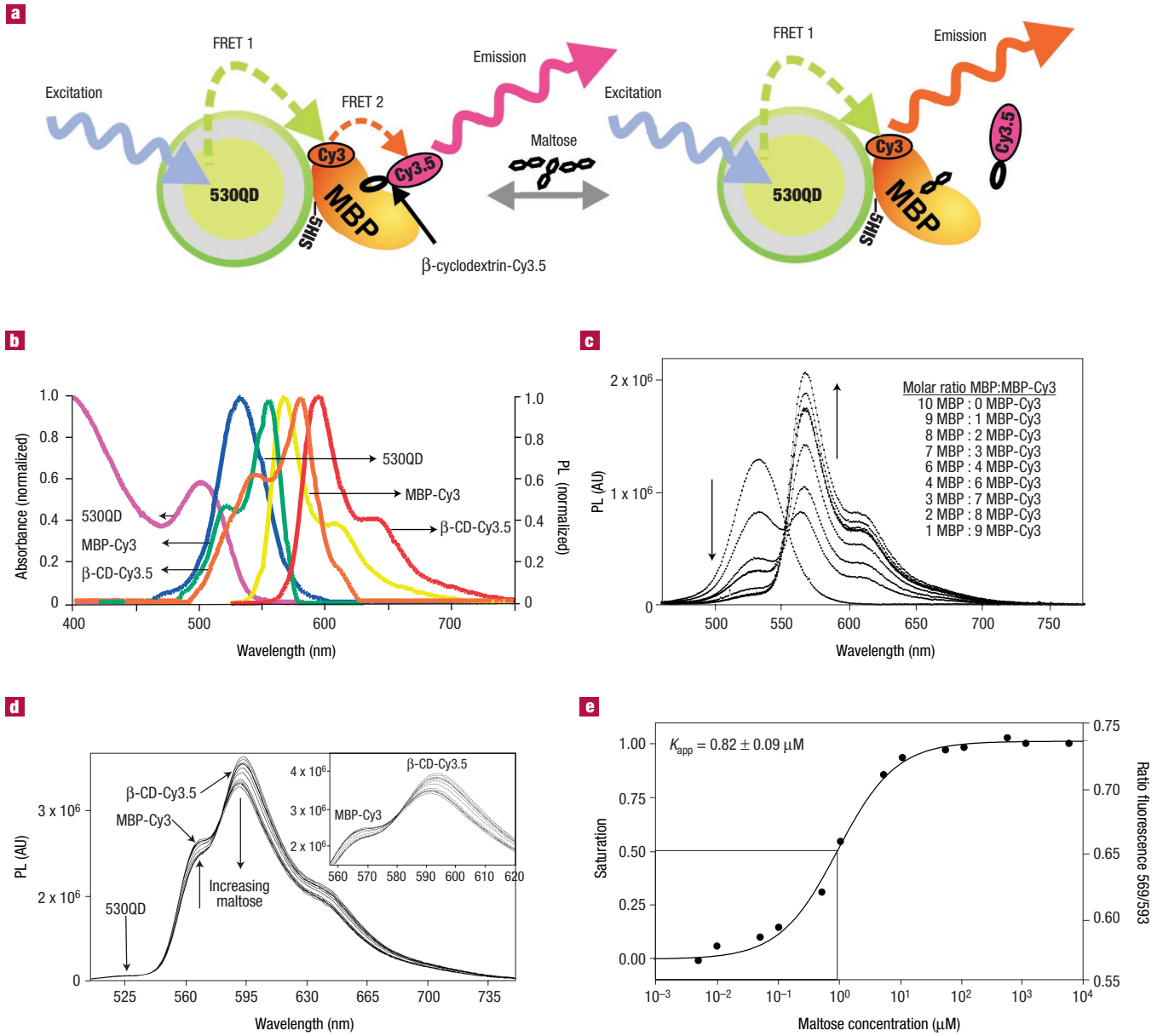

Figure 4 Function and properties of the 530 QD-MBP-Cy3-β-CD-Cy3.5 nanosensor. a, Schematic of a 530QD-MBP-Cy3-β-CD-Cy3.5 maltose sensor assembly. A 530-nm QD is surrounded by ~10 MBPs (only one shown for clarity), each monolabelled with Cy3 at cysteine 95 (maximum absorption ~556 nm, maximum emission ~570 nm). Specifically bound β-CD-Cy3.5 (maximum absorption ~575 nm, maximum emission ~595 nm) completes the QD-10MBP-Cy3-β-CD-Cy3.5 sensor complex. Excitation of the QD results in FRET excitation of the MBP-Cy3, which in turn FRET excites the β-CD-Cy3.5. Added maltose displaces β-CD-Cy3.5 leading to increased Cy3 emission. **b**, Spectral properties of 530QD-MBP-Cy3-β-CD-Cy3.5 sensor assembly. Absorption (pink) and emission spectra (blue) of a 530 QD are displayed along with absorption spectra of MBP-Cy3 (green) and β-CD-Cy3.5 (orange). Emission spectra for MBP-Cy3 (yellow) and β-CD-Cy3.5 (red) are also shown. **c**, 530QD-MBP-Cy3 FRET. 530QDs were conjugated with an increasing ratio of MBPD95C-Cy3 to unlabelled MBP (total MBP/QD constant), and PL was measured at each MBP/MBP-Cy3 ratio as shown (the arrows indicate the increasing ratio). Direct Cy3 dye excitation not subtracted (see Supplementary Information, Fig. S2e,f). **d**, Maltose sensing of 530QD-MBP-Cy3-β-CD-Cy3.5. (Inset) Close-up of the MBP-Cy3 and β-CD-Cy3.5 fluorescence portions. Note the isosbestic point at ~581 nm. A shift of ~4nm in β-CD-Cy3.5 maximum emission was observed for the MBP-Cy3-bound form attributable to bound dye rigidity and inner filtering. **e**, Transformation of titration data. The left axis shows fractional saturation and the right axis shows the ratio of PL at 593 nm/569 nm. Assuming the range of useful measurement to be between 10 and 90% saturation, this translates into a sensing range of ~100 nm to 10 μM maltose[24].

shown in Fig. 4c and the R_0 for the 530-nm QD-Cy3 donor–acceptor pair (48 Å), an average radial distance of ~68 Å from the QD centre to the protein-bound Cy3 position can be estimated (see Methods). This is a distance at which ~15% energy-transfer efficiency should occur for a single-QD–single-Cy3 FRET pair. As before, the presence of several MBP-Cy3 acceptors (~10) associated with each QD contributes significantly to the high overall FRET efficiency (~75% for 10 MBP-Cy3).

With the QD-MBP-Cy3 donor/bridging dye assembly in place, and after formation of the complete nanosensor assembly by occupation of MBP sugar-binding sites with displacable β-CD-Cy3.5, sensitivity to

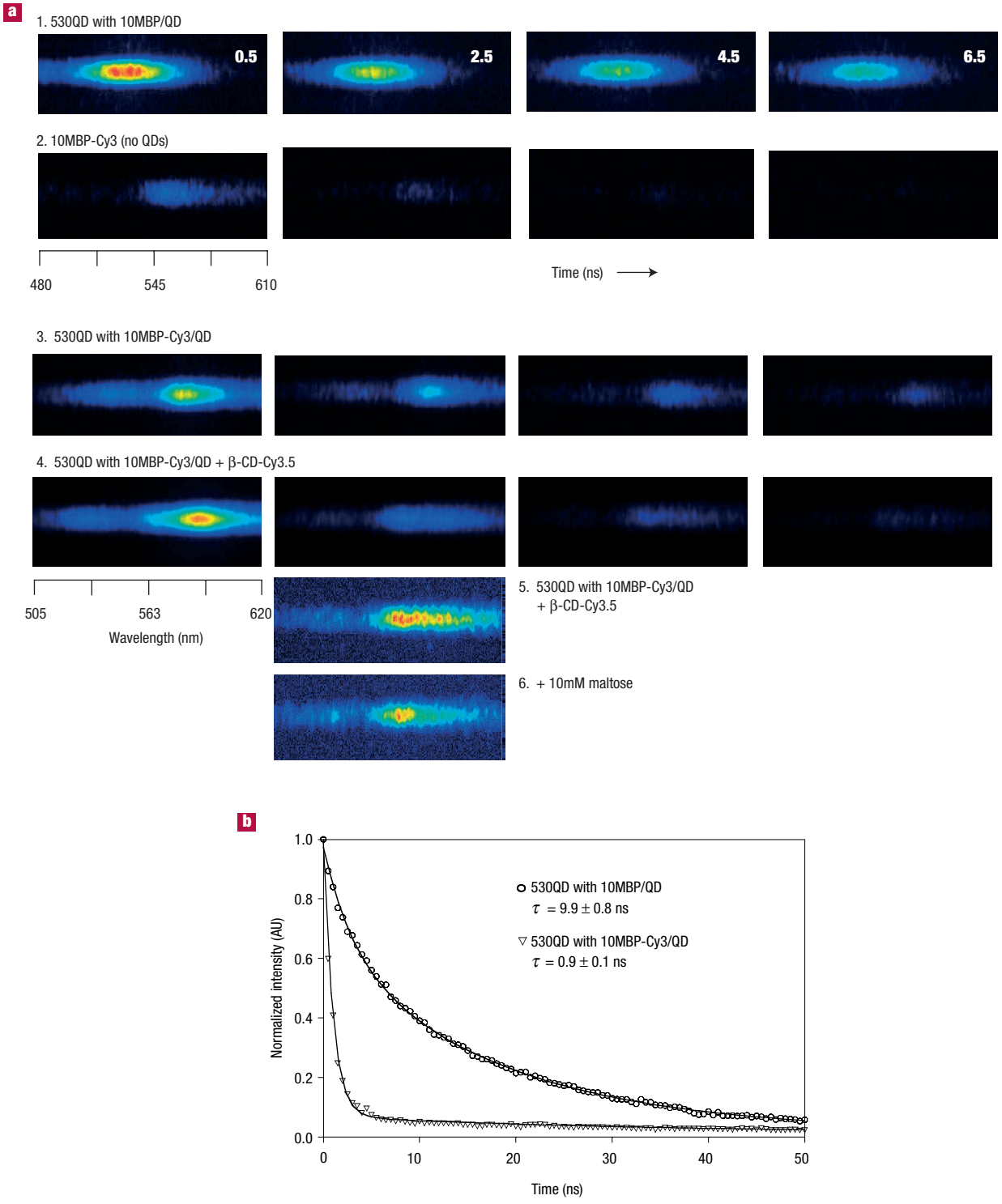

Figure 5 Excited-state properties of the 530QD-MBP-Cy3-β-CD-Cy3.5 nanosensor. a, False colour time-intensity-wavelength images of 530QD-10MBP-Cy3-β-CD-Cy3.5 sensor assembly. Image panel **1**: 530QD-10MBP sensor. Panel **2**: 10MPB-Cy3 (molar amount (~300 picomoles) to coat the 530QDs with 10MPB-Cy3). Panel **3**: 530QD-10MBP-Cy3. Panel **4**: 530 QD-10MBP-Cy3 preloaded with 1 μM β-CD-Cy3.5. Panel **5**: enhanced image of 530QD-10MBP-Cy3-β-CD-Cy3.5 at 2.5 ns and Panel **6**, after the addition of maltose. The appropriate emission wavelength scale is indicated for the panels above and adjacent (intensity: black = 0; blue = lowest; red = highest). **b**, Fluorescence lifetime decay curves and τ values of the 530QD (at λ max) in the 530QD-10MBP and 530QD-10MBP-Cy3 sensor assemblies presented in **a**.

added maltose was demonstrated (Fig. 4d). Under the conditions investigated, a K_{app} of 0.82 ± 0.09 μM for maltose was estimated from titration data (Fig. 4e). This is identical to the binding constant (K_D) value reported for binding of maltose to soluble MBP labelled at position 95 with an acrylodan dye[23]. This value is about tenfold lower than that of the 560QD-based sensor, and this difference can be explained in several ways. The MBP used with Cy3 has an engineered cysteine mutation with this dye attached to it, as opposed to the MBP used with the 560QD sensor. Such modifications can and do have significant effects on MBP binding constants[3,23–25]. Each of these sensors incorporates a different CD–dye adduct which could additionally affect protein recognition. Evidence exists for dyes sequestering themselves inside the CD core, which also may alter binding energetics[34]. Coordination of the MBP to the QD surface may further exacerbate these binding differences. These recognition differences highlight the incomplete nature of our understanding of the molecular-scale energetics and chemical behaviour of QD-surface-bound nanosensor assemblies and point to an important area for further study. Attempts to construct a 'direct', or 'one-step', sensing assembly using the same 530-nm DHLA-QDs conjugated with unlabelled MBP-5HIS acting as receptor for β-CD-Cy3.5/maltose (no FRET relay station) resulted in complexes that were ineffective in sensing maltose (Supplementary Information, Fig. S2d); the level of PL change measured using this 'direct' sensor approached the background noise of our fluorimeter.

To explore the mechanism of steady-state quenching of QD emission observed in 530QD-10MBP-Cy3-β-CD-Cy3.5 nanosensors, fluorescence intensity decay measurements were performed on 530QD-10MBP/QD (unlabelled MBP), 530QD-10MBP-Cy3/QD (Cy3-labelled MBP) and 530QD-10MBP-Cy3/QD-β-CD-Cy3.5 assemblies (Fig. 5a,b). Changes in QD excited-state lifetime for the 530QD-10MBP-Cy3 relay station complexes parallel the results of the steady-state intensity measurements. The average lifetime (τ) for the 530QD-10MBP/QD assemblies is ~10 ns, whereas QD τ was reduced to <1 ns for 530QD-10MBP-Cy3/QD relay station complexes. Data clearly show that excited-state quenching of QDs occurs in concert with a rapid rise in Cy3 emission intensity, as illustrated in two-dimensional time-intensity-wavelength profiles and time versus intensity plots (Fig. 5a,b; Supplementary Information, Fig. S2g). Maltose or β-CD added to 530QD-10MBP complexes had no effect on QD τ values (data not shown). These results demonstrate that a significant portion of QD-emission quenching by bound proteins labelled with the Cy3 relay station fluorophores occurs by resonance energy transfer. As predicted from the 530QD-10MBP-Cy3-β-CD-Cy3.5 (± maltose) system (Fig. 4c,d), addition of β-CD-Cy3.5 to the 530QD-10MBP-Cy3/QD results in a small but distinct decrease in average Cy3 lifetime (from τ ~2.2 ns to τ ~1.9 ns) and Cy3 emission intensity at times of 0.5 ns and longer (Fig. 5a; Supplementary Information, Fig. S2g). Displacement of β-CD-Cy3.5 by excess maltose is observable as a change in the detailed emission profile at 2.5 ns (Fig. 5a bottom) within the overlapping Cy3-Cy3.5 emission region.

We have shown that labelling MBP with dye on almost any residue results in efficient FRET to bound β-CD-dyes due to the small overall MBP size, which yields[25] consistent distance values < R_0. Along with the above data, these results indicate that at least two FRET processes occur. We estimated the FRET relay efficiency of the individual components of this sensor (Supplementary Information)[35]. By comparing the direct-excitation-corrected MBP-Cy3 acceptor emission with 530QD donor PL loss we estimate that ~75% of QD excited state energy in 530QD-10MPB-Cy3 assemblies is transferred to Cy3 through FRET. As the 530QD is ~95% PL-quenched when bound to 10MBP-Cy3, we estimate that FRET accounts for ~71% of this (75% of 95% QD quenching). After correcting for Cy3 and Cy3.5 direct excitation components we estimate that when bound to MBP-Cy3, β-CD-Cy3.5 receives ~20% of the energy of the QDs by FRET, either directly (~6%), or relayed through the ten surrounding MBP-located Cy3 dyes (~14%). This is consistent with the PL changes shown in Fig. 5. Although only one fifth of the energy of the QDs makes it to the β-CD-Cy3.5 by FRET, the more salient point is that at this excitation wavelength this sensor does not function when the QD or the MBP-Cy3 is not present (Supplementary Information, Fig. S2b,d).

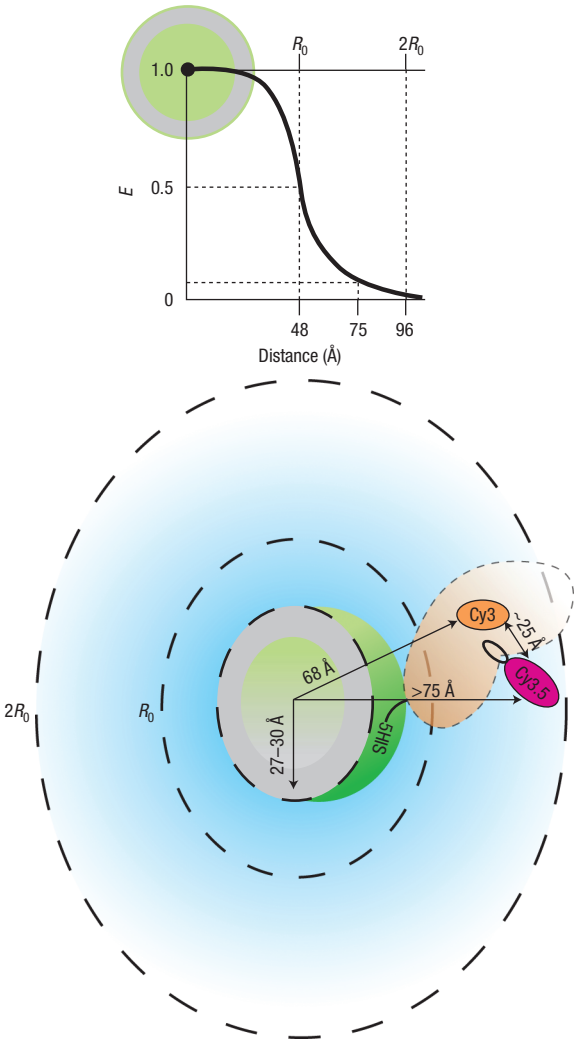

Figure 6 Cutaway schematic depicting critical Förster distances. An idealized core–shell QD emitting at 530 nm is shown. This QD has a CdSe–ZnS radius of 27–30 Å. MBP has dimensions of about[24] 30 × 40 × 65 Å. The Förster radius, R_0, is calculated to be 48 Å for 530QD-MPB-Cy3. The distance from the QD centre to the Cy3 dye located at MBP residue 95C is estimated to be ~68 Å. The plot shows the FRET efficiency, *E*, as a function of distance for this nanosensor, assuming one QD donor to one protein-dye acceptor for simplicity.

From our Cy3 FRET data and the published X-ray coordinates[31] of MBP, predicted donor–acceptor distances involved in the current assemblies can be calculated, and the likely reasons for both the failure of the 530QD-10MBP-β-CD-Cy3.5 direct assembly and the success of the 530QD-10MPB-Cy3-β-CD-Cy3.5 two-step nanosensor can be asserted. Figure 6 schematically describes a plausible scenario in the context of the Förster distances involved in these assemblies (530QD:Cy3.5, the donor–acceptor overlap integral $J(\lambda)$ of 4.61×10^{-13} cm^3 M^{-1} and R_0 = 44.8 Å; 530QD:Cy3, $J(\lambda)$ of 7.01×10^{-13} cm^3 M^{-1} and R_0 = 48.4 Å).

With an estimated 530QD (centre) to MBPD95C-Cy3 distance of ~68 Å, and using ~25 Å for the distance between the Cy3 relay centre and β-CD-Cy3.5 present at the MBP sugar binding site (from the X-ray crystal structure), it is feasible that the dye portion of β-CD-Cy3.5 could bind at least 75 Å (~1.7–1.8 times R_0) from the QD donor centre. For the 'direct' assembly, it appears that the unfavourable combination of this long intra-assembly 530QD donor–MBP-bound β-CD-Cy3.5 acceptor average distance (>75 Å), with a relatively poor donor–acceptor overlap integral for the 530QD-β-CD-Cy3.5 FRET pair, cannot be ameliorated by the combined quenching power provided by the presence of several β-CD-Cy3.5 acceptor moieties specifically bound to each 530QD-10MBP assembly to allow useful sensing. Once the Cy3 FRET 'relay centre' is in place, these deficiencies are partially overcome. The more favourable average QD-Cy3 distance (~68 Å) and the better overlap integral for 530QDs and Cy3 allow the dye to function in its intended 'relay station' role. Indeed, the presence of this relay boosts the energy that the MBP-Cy3-bound β-CD-Cy3.5 receives through FRET by more than threefold (~6% to ~20%). Even with a FRET 'relay' dye present, energy transfer is relatively inefficient (Supplementary Information, Table S2). More optimal placement of the bridging dye could be achieved through further structure-informed protein engineering to improve this two-step FRET nanosensor system. Although we have used a protein-bound MPB-Cy3 energy-transfer relay to overcome donor–acceptor distance limitations, it is possible that direct modification of nanocrystal surfaces with appropriate bridging dyes could yield efficient relay donors that take advantage of QD optical properties but have less-rigid Förster distance constraints.

In contrast to the ineffective 530QD-10MBP-β-CD-Cy3.5 direct'assembly, the 560QD-10MBP-β-CD-QSY9 direct sensor assembly is functional due to a combination of the higher quantum yield of the 560QD-MBP conjugate (by >2.5-fold, 15% versus 39%) and the more favorable $J(\lambda)$ of 6.3×10^{-13} cm^3 M^{-1} yielding R_0 of 56.5 Å. For both the 560QD-10MBP-β-CD-QSY9 and 530QD-10MBP-Cy3-β-CD-Cy3.5 assemblies, the quantitative effect on FRET efficiency (E) of having multiple acceptors for each QD donor can be estimated from the formula $E = nR_0^6/nR_0^6 + r^6$, where r is the average donor–acceptor radius. For example, with $R_0 = 56$ Å and $r = 70$ Å, changing from $n = 1$ to $n = 5$ energy acceptors should result in enhancement of E from ~20 to 55%. This is consistent with our observations of the 560QD-10MBP-β-CD-QSY9, assuming that the 10 MBP surrounding each QD are >50% saturated with β-CD-QSY9 at the concentrations used.

Considerable control over the protein-to-QD ratio in the sensor self-assembly process can be achieved using oligohistidine-directed attachment of a protein biorecognition element to the ZnS-DHLA QD surface. Engineered oligohistidine sequences are usually well tolerated at either terminus, or even within the primary sequence, of many proteins, and serve as the basis for easy purification using immobilized metal affinity chromatography[36]. We have conjugated DHLA-QDs with other oligohistidine-tagged proteins and this binding has resulted in comparable levels of surface-saturable PL enhancement (data not shown). Should this means of QD–protein conjugation turn out to be generally applicable, the ready availability of many oligohistidine-labelled proteins and the ease of their engineering will allow ready assembly of diverse types of QD–protein-based nanosensors. Using this method, formation of QD–protein assemblies with multiple copies of more than one kind of protein on each QD surface can be accomplished[10,11], which will make possible the design and construction of other (sensor or non-sensor related) hybrid materials with considerable structural and functional complexity.

Besides the QD surface protection/solubilization by DHLA that we have used, there are several alternative methods for passivating/activating CdSe–ZnS QD surfaces[9,12,14,16,37–39]; however as the thickness of any passivating/activating surface layer increases, inherent donor–acceptor Förster distance constraints affecting FRET will become increasingly pronounced. Other useful receptors for building nanoassemblies using QD FRET donors include DNA, RNA, PNA, peptides, recombinant antibodies and antibody fragments, and small molecules such as drugs. Whole IgG antibodies may be difficult to use directly due to their large size in the light of donor–acceptor distance constraints. Optimization of system variables, donor–acceptor $J(\lambda)$ and the number of acceptors per QD, will be critical for successful signal transduction.

MBP undergoes a significant conformational change on binding of maltose[5,22,23]. In the present MBP-based FRET sensors where signal transduction occurs solely due to displacement of β-CD-dye derivatives from the MBP site, conformational changes that result from maltose binding are optically silent. In addition to the displacement-based FRET sensing mode we used, other types of QD nanosensors that are responsive to sugar binding could be developed. Implantation of energy acceptors at appropriate conformationally mobile sites within MPB should allow construction of 'reagentless' FRET sensors having fixed QD donor elements.

In this report, we have described preparation and testing of the first well-characterized QD-protein/receptor inorganic nanocrystal–biomolecule nanosensor assemblies. We have demonstrated that biologically compatible QDs can act as FRET donors in recognition-based sensing. The ability to conjugate each QD FRET donor with a relatively large number of quasi-symmetrically arranged specific receptors presents an exciting opportunity for construction and optimization of new types of optically addressed nanosensors. These include assemblies with mixed surfaces for multiplexed sensing, improved optical sensors for intracellular monitoring, or complex biomimetic light harvesting devices[3,4,40]. The unique and robust optical properties of QDs, together with the novel features of their biomolecular conjugates, should result in sensors and nanostructures with important applications in a variety of areas, including healthcare, environmental monitoring and biodefence.

METHODS

ASSEMBLY AND TESTING OF QD–MBP SENSORS

The MBP-5HIS protein was purified as described elsewhere[3,7,25]. DHLA QDs[7] and β-CD-dye adducts[25] were prepared as described elsewhere. For each self-assembly and fluorimetry experiment, 30 pmol of QD was used. 560QD-10 MBP/QD-β-CD-QSY9 nanosensor assembly: 1 μM β-CD-QSY9 was mixed with the appropriate amount of MBP-5HIS (the amount required to coat each QD with 10 MBPs/QD) and allowed to bind in a concentrated form (ratio of β-CD-dye to MBP was ~10:1). This was mixed with 30 pmol of QD in 50 μl 10 mM NaCl, 10 mM Na-tetraborate buffer (pH 9.55) for 1 h to allow self-assembly of the QD-MBP-β-CD nanosensor (530-QD-10MBP-Cy3/QD-β-CD-Cy3.5 nanosensor: same procedure with appropriate substitutions). Concentrated assemblies were diluted into 3 ml borate buffer in a cuvette for assaying. Data was collected using a SPEX Fluorolog-2 Fluorimeter (Jobin Yvon/SPEX, Edison, New Jersey) with excitation at 450 nm (close to a Cy3 absorption minimum) and emission monitored at right angles with slit widths set at 2–5 nm. Maltose concentrations added in titrations were: 5 nM, 10 nM, 50 nM, 100 nM, 500 nM, 1 μM, 5 μM, 10 μM, 50 μM, 100 μM, 500 μM, 1 mM, 5 mM, 10 mM. Solutions were allowed to equilibrate for 5 min between maltose additions while stirring at constant temperature (22 °C); these additions altered the final volume by <3%. Lifetime data was collected on a far-field epifluorescence microscope (in-house construction) coupled to a spectrometer (Jobin-Yvon Triax320) and time-gated microchannel plate-intensified CCD camera (Labvision, Picostar Images). A GaN diode laser (414 nm, 5 MHz, 90 ps FWHM, PicoQuant GmBH, LDH400) with excitation power of ~30 μW was used. Excitation light was coupled into the microscope collection axis using a 400-nm dichroic filter and a 0.3 NA Nikon ×10 air objective for both focusing and collection. Experiments were performed at room temperature with 100 pmol QD ml^{-1}. Raw data was collected as wavelength intensity versus time plots and processed using DaVis software (LaVision GmBH). Data was fitted in Matlab using a stretch exponential[41]. False colour images were derived from the CCD camera at discrete timepoints following the laser excitation pulse, and are scaled representations of the intensity levels as a function of wavelength.

DATA ANALYSIS

Fluorescence data was corrected for inner filtering where necessary[26]. Maltose titration data was fit to a four-parameter Hill equation in SigmaPlot. The point corresponding to 50% saturation derives the K_{app}. For all titrations the Hill coefficient approached 1, indicating a 1:1 maltose/MBP interaction. All values are derived from the average of at least three titrations. Lifetime data was fitted to a stretch exponential using fminsearch in Matlab (a simplex minimization routine). Stretch exponentials account for a distribution of lifetime values in the ensemble. We used the distribution's average lifetime in our FRET analyses, calculated as[41] $\langle\tau\rangle = \tau/\beta \times \Gamma(1/\beta)$.

QUANTUM YIELD, R_0 AND FRET EFFICIENCY

Quantum yields were determined as described elsewhere[26]. R_0 values were estimated using the formula $R_0 = 9.78 \times 10^3 [\kappa^2 n^{-4} Q_D J(\lambda)]^{1/6}$ where $\kappa^2 = 2/3$, n is the refractive index of the medium, Q_D is the quantum

yield of the donor in the absence of acceptor and $J(\lambda)$ is the overlap integral[26]. Average radii, r, from QD centre to FRET acceptors was calculated using efficiency:

$$E_c = 1 - \frac{F_{DA}}{F_D} = \frac{nR_0^6}{nR_0^6 + r^6}$$

(n = number of MBP-Cy3/QD)[26],

and then distance:

$$r_n = \left[\frac{nR_0^6 (1 - E_c)}{E} \right]$$

where F_D is the relative fluorescence of the donor in the absence of acceptor and F_{DA} in the presence of acceptor. As no FRET process is 100% efficient, an estimate of efficiency ($E \times c$; where c = corrected) was made from corrected acceptor emission enhancement. E_c is this adjusted value and the r distances account for this where possible. For the 530QD donor to 10 MBP-Cy3 FRET, the estimate is ~75% of energy emitted by the donor is transferred to the acceptor by FRET.

Received 15 April 2003; accepted 21 July 2003; published 24 August 2003.

References

1 Iqbal, S. S. *et al.* A review of molecular recognition technologies for detection of biological threat agents. *Biosens. Bioelect.* **15,** 549–578 (2000).
2. O'Connell, P. J. & Guilbault, G. G. Future trends in biosensor research. *Anal. Lett.* **34,** 1063–1078 (2001).
3. De Lorimier, R. M. *et al.* Construction of a fluorescent biosensor family. *Protein Sci.* **11,** 2655–2675 (2002).
4. Scheller, F. W., Wollenberger, U., Warsinke, A., & Lisdat, F. Research and development in biosensors. *Curr. Opin. Biotech.* **12,** 35–40 (2001).
5. Hellinga, H. W. & Marvin, J. S. Protein engineering and the development of generic biosensors. *Trends Biotech.* **16,** 183–189 (1998).
6. Benson, D. E., Conrad, D. W., de Lorimer, R. M., Trammel, S. A. & Hellinga, H. W. Design of bioelectronic interfaces by exploiting hinge-bending motions of proteins. *Science* **293,** 1641–1644 (2001).
7. Mattoussi, H. *et al.* Self-Assembly of CdSE-ZnS quantum dot bioconjugates using an engineered recombinant protein. *J. Am. Chem. Soc.* **122,** 12142–12450 (2000).
8. Bruchez, M., Moronne, J. M., Gin, P., Weiss, S. & Alivisatos, A. P. Semiconductor nanocrystals as fluorescent biological labels. *Science* **281,** 2013–2018 (1998).
9. Chan, W. C. W. & Nie, S. Quantum dot bioconjugates for ultrasensitive nonisotopic detection. *Science* **281,** 2016–1028 (1998).
10. Goldman, E. R. *et al.* Conjugation of luminescent quantum dots with antibodies using an engineered adaptor protein to provide new reagents for fluoroimmunoassays. *Anal. Chem.* **274,** 841–847 (2002).
11. Goldman, E. R. *et al.* Avidin: A natural bridge for quantum dot-antibody conjugates. *J. Am. Chem. Soc.* **122,** 6378–6382 (2002).
12. Dubertret, B. *et al.* In vivo imaging of quantum dots encapsulated in phospholipid micelles. *Science* **298,** 1759–1761 (2002).
13. Jaiswal, J. K., Mattoussi, H, Mauro, J. M. & Simon, S. M. Long-term multiple color imaging of live cells using quantum dot bioconjugates. *Nature Biotech.* **21,** 47–51 (2003).
14. Mattoussi, H, *et al.* in *Optical Biosensors: Present and Future* (eds Ligler, F. S. & Rowe Taitt, C. A.). (Elsevier, The Netherlands, 2002).
15. Akerman, M. E. *et al.* Nanocrystal targeting in vivo. *Proc. Natl Acad. Sci. USA* **99,** 12617–12621 (2002).
16. Wu, X. Y. *et al.* Immunofluorescent labeling of cancer marker Her2 and other cellular targets with semiconductor quantum dots. *Nature Biotech.* **21,** 41–46 (2003).
17. Kagan, C. R., Murray, C. B. & Bawendi, M. G. Long-range resonance transfer of electronic excitations in close-packed CdSe quantum-dot solids. *Phys. Rev. B* **54,** 8633–8643 (1996).
18. Kagan, C. R., Murray, C. B. Nirmal, M. & Bawendi, M. G. Electronic energy transfer in CdSe quantum dot solids. *Phys. Rev. Lett.* **76,** 1517–1520 (1996).
19. Crooker, S. A., Hollingsworth, J. A., Tretiak, S. & Klimov, V. I. Sprectrally resolved dynamics of energy transfer in quantum-dot assemblies: towards engineered energy flows in artificial materials. *Phys. Rev. Lett.* **89,** 186802 (2002).
20. Willard, D. M., Carillo, L. L., Jung, J. & Van Orden, A. CdSe-ZnS Quntum Dots as resonance energy transfer donors in a model protein-protein binding assay. *Nano Lett.* **1,** 469–474 (2001).
21. Wang, S., Mamedova, N, Kotov, N. A., Chem, W. & Studer, J. Antigen/antibody immunocomplex from CdTE nanoparticle bioconjugates. *Nano Lett.* **2,** 817–822 (2002).
22. Gilardi, G., Zhou, L. Q., Hibbert, L. & Cass, A. E. Engineering the maltose binding protein for reagentless fluorescence sensing. *Anal. Chem.* **66,** 3840–3847 (1994).
23. Marvin, J. S. *et al.* The rational design of allosteric interactions in a monomeric protein and its applications to the construction of biosensors. *Proc. Natl Acad. Sci. USA* **94,** 4366–4371 (1997).
24. Fehr, M., Frommer, W. B. & Lalonde, S. Visualization of maltose uptake in living yeast cells by fluorescent nanosensors. *Proc. Natl Acad. Sci. USA* **99,** 9846–9851 (2002).
25. Medintz, I. L., Goldman, E. R., Lassman, M. E. & Mauro, J. M. A fluorescence resonance energy transfer sensor based on maltose binding protein. *Bioconj. Chem.* (in the press).
26. Lakowicz, J. R. *Principles of Fluorescence Spectroscopy* 2nd edn (Kluwer Academic, New York, 1999).
27. Flora, B., Gusman, H., Helmerhorst, E. J., Troxler, R. F. & Oppenheim, F. G. A new method for the isolation of histatins 1, 3, and 5 from parotid secretion using zinc precipitation. *Protein Expr. Purif.* **23,** 198–206 (2001).
28. Mamedova, N. N., Kotov, N. A., Rogach, A. L. & Studer, J. Albumin-CdTe nanoparticle bioconjugates: preparation, structure, and interunit energy transfer with antenna effect. *Nano Lett.* **1,** 281–286 (2001).
29. Wang, L. Y., Kan, X. W., Zhang, M. C., Zhu, C. Q. & Wang, L. Fluorescence for the determination of protein with functionalized nano-ZnS. *The Analyst* **127,** 1531–1534 (2002).
30. Hanaki, K. *et al.* Semiconductor quantum dot/albumin complex is a long-life and highly photostable endosome marker. *Biochem. Biophys. Res. Comm.* **302,** 496–501 (2003).
31. Sharff, A. J., Rodseth, L. E. & Quicho, F. A. Refined 1.8 Å structure reveals the mode of binding of β-cyclodextrin to the maltodextrin binding protein. *Biochemistry* **32,** 10553–10559 (1993).
32. Kawahara, S., Uchimaru, T. & Murata, S. Sequential multistep energy transfer: enhancement of efficiency of long-range fluorescence resonance energy transfer. *Communication* **6,** 563–564 (1999).
33. Tong, A. K., Li, Z., Jones, G. S., Russon, J. J. & Ju, J. Combinatorial fluorescence energy transfer tags for multiplex biological assays. *Nature Biotech.* **19,** 756–759 (2001).
34. Guether, R. & Reddington, M. V. Photostable cyanine dye β–cyclodextrin conjugates. *Tetrahedr. Lett.* **38,** 6167–6170 (1997).
35. Watrob, H. M., Pan, C. P. & Barkley, M. D. Two-step FRET as a structural tool. *J. Am. Chem. Soc.* **125,** 7336–7343 (2003).
36. Schafer, F. *et al.* Automated high-throughput purification of 6XHis-tagged proteins. *J. Biomol. Tech.* **13,** 131–137 (2002).
37. Pathak S. *et al.* Hydroxylated quantum dots as luminescent probes for in situ hybridization. *J. Am. Chem. Soc.* **123,** 4103–4104 (2001).
38. Gerion, D. *et al.* Sorting fluorescent nanocrystals with DNA. *J. Am. Chem. Soc.* **124,** 7070–7074 (2002).
39. Guo, W., Li, J. J., Wang, Y. A. & Peng, X. Luminescent CdSe/CdS core/shell nanocrystals in dendron boxes:superior chemical, photochemical and thermal stability *J. Am. Chem. Soc.* **125,** 3901–3909 (2003).
40. Willner, I., Patolsky, F. & Wasserman, J. Photoelectrochemistry with controlled DNA-cross-linked CdS nanoparticle arrays. *Angew. Chem. Int. Edn Engl.* **40,** 1861–1864 (2001).
41. Lindsey, C. P. & Pattersson, G. D. Detailed comparison of the Williams-Watts and Cole-Davidson functions. *J. Chem. Phys.* **73,** 3348–3357(1980).

Acknowledgements

The authors thank H. Hellinga and D. Conrad (Duke University) for providing the plasmid with the MBP-HIS-tagged gene sequence used and P.T. Tran for helpful insight. I.L.M. and A.R.C. are supported by National Research Council Fellowships through the Naval Research Laboratory. B.F. acknowledges the National Defense Science and Engineering Graduate Fellowship Program for support. H.M., E.R.G. and J.M.M acknowledge K. Ward at the Office of Naval Research (ONR) for research support and grant number N001400WX20094 for financial support. The views, opinions, and/or findings described in this report are those of the authors and should not be construed as official Department of the Navy positions, policies, or decisions.

Correspondence and requests for materials should be addressed to J.M.M. or H. M.

Supplementary Information accompanies the paper on www.nature.com/naturematerials

Competing financial interests

The authors declare that they have no competing financial interests.